CRYSTAL GROWTH & DESIGN

Article

pubs.acs.org/crystal

Template-Assisted Crystallization of Sulfates onto Calcite: Implications for the Prevention of Salt Damage

E. Ruiz-Agudo,*[,†] C. V. Putnis,[‡] L. Pel,[§] and C. Rodriguez-Navarro[†]

[†]Departamento de Mineralogia y Petrologia, Universidad de Granada, Fuentenueva s/n, 18002 Granada, Spain

[‡]Institut für Mineralogie, Universität Münster, Corrensstrasse 24, 48149 Münster, Germany

[§]Department of Physics, Eindhoven University of Technology, P. O. Box 513, 5600 MB Eindhoven, The Netherlands

ABSTRACT: In situ X-ray diffraction (XRD) and environmental scanning electron microscope (ESEM) crystallization experiments show oriented growth of magnesium sulfate crystals on a diethylenetriamine-penta-methylene phosphonic acid (DTPMP) template adsorbed onto Iceland spar (calcite, $CaCO_3$) cleavage surfaces. Epsomite ($MgSO_4{\cdot}7H_2O$) and hexahydrite ($MgSO_4{\cdot}6H_2O$) crystallize (depending on the ambient conditions) in the presence of DTPMP with $(010)_{epsomite}//(10\bar{1}4)_{calcite}$ and $(\bar{1}11)_{hexahydrite}//(10\bar{1}4)_{calcite}$, whereas in the absence of DTPMP they show no preferred orientation. On the other hand, sodium sulfate (mirabilite, $Na_2SO_4{\cdot}10H_2O$) nucleates onto a Ca-DTPMP precipitate with $(001)_{mirabilite}//(10\bar{1}4)_{calcite}$. In contrast, different sodium sulfate phases crystallize and grow with no preferred crystallographic orientation in the absence of an organic additive. These results allow us to propose a model for the interaction calcite-DTPMP-Na and Mg sulfates based on the template-assisted nucleation and oriented heterogeneous crystallization, mediated by a Ca-precipitate, of inorganic salts on calcitic substrates. This effect results in a (measured) reduction in the critical supersaturation reached by these salts when crystallizing in confined geometries, i.e., a pore, thus resulting in a reduction in crystallization pressure and damage to porous substrates such as building stones. These results have implications in fields where in-pore crystallization of salts results in damage or plugging of the porous network, e.g., cultural heritage conservation and in the oil industry, where phosphonates are used as crystallization inhibitors.

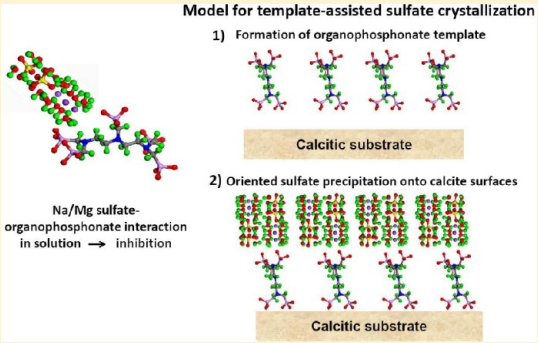

INTRODUCTION

Organic substances are known to play a critical role in the crystallization of inorganic phases.[1] Even when present in very low concentrations, they have a profound impact on crystal shape, size, and polymorph selection of a range of minerals, including carbonates, oxalates, phosphates and sulfates.[2−8] The controlled crystallization of these phases is of industrial and technological importance (e.g., scale control).[9,10] It is also important in biomineralization[11,12] and pathological mineralization,[13,14] as well as in the design of novel biomimetic materials.[15] Organic additives can promote or inhibit crystal growth.[16,17] The catalytic (promoter) effect of additives on crystallization from supersaturated solutions is generally related to two-dimensional (2D) and/or three-dimensional (3D) heterogeneous nucleation.[18] Crystallization inhibition is commonly attributed to step blocking or growth site poisoning by additive adsorption on crystal surfaces. Additive molecules may adsorb on all crystal faces thus reducing the overall growth rate to zero (nucleation inhibitors) or on specific faces (habit modifiers) leading to a change in crystal morphology.[19,20] Crystallization inhibitors have been employed in industry to prevent salt scaling and pipe blocking,[10,21,22] to control polymorphism and crystal size in the pharmaceutical industry,[21] or to inhibit cement hydration[23] and delay gypsum plaster setting.[24]

There is evidence that, in many cases, solid substrates promote heterogeneous crystal nucleation.[25] The inductive effect of substrates on crystal nucleation and growth is generally considered to be related to structural fit between the overgrowth and the underlying matrix.[26] A high structural fit may result in epitaxy. When there is a structural mismatching between substrate and overgrowth, the presence of organic templates may help couple both structures.[25] This has important advantages, and epitaxial crystallization techniques involving the use of self-organized substrates to regulate crystal nucleation and growth are employed in the laboratory and in industry to control size, habit and orientation of crystals.[26−28] In nature, organic templates are known to direct the nucleation and growth of inorganic phases during biomineralization.[12,29−33] Knowledge gained from the study of biomineralization has been applied for the template-directed "biomimetic" production of a range of minerals with controlled morphology, size and orientation (see review by Meldrum and Cölfen[15]).

Despite the widespread presence both in industry and in nature of substrate-mediated crystallization processes, there are numerous effects of the organized substrate on crystal

Received: May 31, 2012
Revised: November 16, 2012
Published: November 16, 2012

 © 2012 American Chemical Society

nucleation and growth which are not yet fully understood, including changes in the crystallizing phase and polymorph and in the supersaturation reached at the onset of crystallization. These aspects are of particular interest when crystallization takes place in confined geometries. The growth of salt crystals in a confined space (pore) is known to exert a pressure against the pore wall which can exceed the rupture modulus of most ornamental materials, often leading to their fracture and crumbling.[34,35] This is one of the main factors causing rock decay in nature[34,36] and weathering of stone buildings and other engineering structures.[37−39] The crystallization pressure exerted by a crystal when growing within a pore has been related both to the degree of supersaturation in a solution and to the properties of curved interfaces between the crystal and the solution (i.e., properties of the material pore system).[35,40] New strategies to prevent salt damage to porous stone based on the use of crystallization inhibitors have been proposed.[41−43] In solution, these compounds increase induction time and critical supersaturation (i.e., the supersaturation reached at the onset of crystallization), thus allowing transport of the saline solution to the surface of the porous stone where salt crystallization eventually precipitates as harmless efflorescence. For this purpose, phosphonates, phosphates and polyphosphates, carboxylic acid derivatives, polyacrylates and ferrocyanides have been tested (see Ruiz-Agudo et al.[44] and refs therein). Most of the additives used widely to inhibit crystallization in technological and industrial applications are polyelectrolytes with a strong tendency to adsorb on a wide range of mineral surfaces. For example, phosphonates are known to adsorb on silica and clays, barite, cassiterite, aluminum oxides, iron oxides, gypsum and calcite.[45−47] In fact, adsorption/precipitation of Ca-phosphonate phases in carbonate reservoirs has been proposed as a means for the slow release of phosphonate ions to inhibit scale formation in porous media.[48] Therefore, it is expected that the effect of such organic molecules on salt crystallization will change noticeably in the presence of an inorganic support (i.e., a porous stone).

Here we study the crystallization of sodium and magnesium sulfates in the presence of an inorganic substrate (calcite), directed by organic molecules (DTPMP, diethylenetriamine-pentakis (methylphosphonic acid)). Mg- and Na-sulfates are extensively found in both modern cement structures and in the stone built heritage. There are numerous examples of the weathering of rock outcrops and ornamental stone associated with the presence of these salts (see review by Goudie and Viles[49]). Both are extremely damaging and show different crystallization patterns.[50] These factors have made Mg- and Na-sulfates the choice for building materials accelerated decay testing.[39,51] The organophosphonate compound DTPMP is known for its inhibitory effect on both the precipitation of sodium and magnesium sulfate when the DTPMP molecules are free in solution.[44,52] The aim of this paper is to combine both macroscale (X-ray diffraction, XRD, and nuclear magnetic resonance, NMR) and microscale (atomic force microscopy, AFM; environmental scanning electron microscopy, ESEM) in situ techniques for on-line monitoring of the crystallization of sodium and magnesium sulfates on Iceland Spar (calcite, $CaCO_3$) single crystals and within limestone blocks in the presence of DTPMP, in order to gain a better understanding of the phosphonate-directed crystallization of inorganic salts onto calcite. The gained knowledge may have direct application in a wide range of fields where the presence of saline solutions and organic molecules may result in template-assisted crystal growth within porous materials, including cultural heritage conservation, scale formation in the oil and cement industry and biomineralization.

■ MATERIALS AND METHODS

(a). Salt Solutions, Additives and Calcitic Substrates. Na and Mg sulfate saturated solutions were prepared using anhydrous solids (Panreac, analytical grade) and deionized water. DTPMP (Fluka, reagent grade) was added to the solutions in concentrations ranging from 10^{-4} M to 10^{-2} M. Solution pH was adjusted to 8 using NaOH solution as needed depending on the additive concentration. The ability of an organophosphonate molecule to be adsorbed on a crystal surface depends on its ability to be attracted to the surface and bonded to it. With increasing pH, the phosphonate groups of DTPMP will be increasingly deprotonated and thus the ability of the molecule to interact with the surface will increase. At pH 8, DTPMP is already highly deprotonated (eight negative charges). This alkaline pH will also prevent a massive dissolution of calcite. In order to increase the degree of deprotonation, the pH should be significantly higher and thus working at higher pH values was discarded. Two different calcitic supports were used to study the crystallization of sulfates in the presence of DTPMP: (i) freshly cleaved Iceland Spar single crystals (ca. 2 × 3 × 5 mm sized) and (ii) blocks (3 × 3 × 25 cm sized) of a porous biomicritic limestone (Santa Pudia quarries, Escúzar, Granada). DTPMP adsorption experiments were performed using calcite powders (Sigma-Aldrich, ACS reagent). This powder is essentially pure calcite (as determined by X-ray diffraction and X-ray fluorescence), and the BET specific surface area measured by nitrogen adsorption (Micromeritics TriStar) was found to be 1.46 ± 0.02 $m^2 \cdot g^{-1}$.

(b). DTPMP Uptake by Calcite Powder. The uptake of DTPMP by calcite was investigated using calcite powder, following the method described by Xyla et al.[53] DTPMP solutions of variable concentration were prepared from the corresponding stock solution of pure solid reagent. Solutions were placed in screw-capped polyethylene vials, and their pH was adjusted to 8 by the addition of very small amounts of NaOH. Next, calcite powders were immersed in the solutions in amounts enough to provide a total surface area of 0.2 m^2. The vials were sealed and placed in a chamber thermostatted by circulating water at 25.0 + 0.5 °C for 2 h. The organophosphorous content in the supernatant was analyzed by digestion with potassium persulfate, according to the method outlined by Grasshoff et. al.[54] Magnesium and sodium sulfate were used as background electrolyte in the adsorption experiments, which were carried out at two different ionic strengths (0.1 and 2).

(c). Nanoscale Observations of Saline Solution−DTPMP−Calcite Interactions. In situ nanoscale observations of the $\{10\bar{1}4\}$ calcite surfaces during contact with saline solutions in the presence/absence of DTPMP were performed using a fluid cell of a Digital Instruments Nanoscope III Multimode AFM working in contact mode. The scanning frequency was 5 Hz, and the areas scanned were mostly 5 × 5 and 10 × 10 μm. AFM images were collected using Si_3N_4 tips (Veeco Instruments, tip model NP-S20) with spring constants 0.12 N/m and 0.58 N/m. Images were analyzed using the NanoScope software (Version 5.12b48). Saturated magnesium and sodium sulfate solutions with and without 30 mM DTPMP flowed continuously for 30 min at a rate of 50 $mL \cdot h^{-1}$ from a syringe coupled to an O-ring-sealed fluid cell containing the sample crystal. Before each experiment, deionized water and standard growth solution (0.3 mM $CaCl_2$ and Na_2CO_3 giving a supersaturation index 0.81 calculated using PHREEQC[55]) were passed over the crystal to clean the cleaved surface, as well as to adjust the AFM parameters as in Arvidson et al.[56]

(d). In Situ XRD and ESEM Experiments on Calcite Single Crystals. Calcite $\{10\bar{1}4\}$ surfaces were used as substrates. Prior to each experiment, rhombohedral fragments, ca. 5 × 3 × 2 mm in size, were freshly cleaved with a knife blade from single crystals of optical quality Iceland Spar. They were examined by optical microscopy to ensure that cleavage surfaces were free from macroscopic steps and small particles. Drops of saline solution were deposited and let to

crystallize onto these surfaces. Supersaturation was achieved by evaporation at constant temperature (16 ± 1, 20 ± 1 or 25 ± 1 °C) and relative humidity (40 ± 5 or 50 ± 6%) within the chamber of a Philips PW-1710 diffractometer equipped with an automatic slit. XRD measurement parameters were CuKα radiation (λ = 1.5405 Å), an exploration range of 10−50° 2θ, steps of 0.028° 2θ, and a goniometer speed of 0.01° 2θ s^{-1}. XRD patterns were collected at 4 min intervals, while evaporation and the eventual crystallization of the salt were taking place on the Iceland spar crystal. Analysis of the relative intensity of the main Bragg peaks was performed using the XPowder software package in order to identify which faces were preferentially developed (with a preferred crystallographic orientation) in the presence of the additive on the calcite substrate. Habit and size distribution of sodium and magnesium sulfate crystals precipitated from drops of saline solution deposited onto Iceland Spar crystals were studied using a Philips Quanta 400 ESEM. In this case, supersaturation was achieved by modifying the gas pressure (pH_2O) inside the ESEM chamber from 6.5 to 3.5 Torr, at a rate of 0.01 Torr·s^{-1}, and keeping constant the temperature (2 °C), following the methodology outlined by Rodriguez-Navarro and Doehne.[39]

(e). Study of Salt Crystallization within a Porous Calcitic Support. Macroscale crystallization tests were performed using limestone prisms (3 × 3 × 25 cm) from Santa Pudia quarry (Granada, Spain) (see Ruiz-Agudo et al.[52] for details on this stone type), by allowing saturated saline solution to flow through the stone, evaporate, and crystallize. This test simulates conditions of capillary rise and salt damage to the walls of historical buildings.[39] Details of the experimental set up are given in Rodríguez-Navarro et al.[43] Salt crystallization occurred following evaporation of the solution with and without addition of 1 mM DTPMP. The evaporation rate was monitored by on line weight measurements. Eventual efflorescence development and damage to the stone support were monitored by digital photographs. Changes in the stone pore system after salt crystallization tests were studied using mercury intrusion porosimetry (MIP) on a Micromeritics Autopore (details on sample preparation and analysis are given in Ruiz-Agudo et al.[52]).

Quantitative measurements of moisture distribution and salt concentration during saline solution evaporation and crystallization within limestone pores were performed with a high spatial resolution using nuclear magnetic resonance (NMR). These measurements were done using equipment especially designed for measurements on porous materials (see Kopinga and Pel[57] for details). This apparatus uses a conventional iron-cored electromagnet, generating a field of 0.7 T. Samples for measurements have a cylindrical shape with a diameter of 20 mm and a length of 45 mm, and are moved vertically through the magnet with the help of a step motor. The samples are capillary saturated with a 1 M Na_2SO_4 solution, sealed on all sides (except for the top) and dried at 20 °C and 5% relative humidity. It takes 2 h to measure a moisture and ion profile. Home-built Anderson gradient coils were employed, yielding magnetic field gradients in one spatial direction of up to 0.3 T/m, resulting in a one-dimensional resolution on the order of 1.0 mm for the material investigated. The apparatus is designed in a way that quantitative measurements can be performed (unlike standard magnetic resonance imaging, MRI, which is generally used in a qualitative way). This requires a specially designed Faraday shield that is placed between the RF coil and the sample, to suppress the effects of changes in dielectric permittivity by variations in moisture content. By a computer-controlled switch the LC circuit of the insert can be tuned to 33 MHz (hydrogen resonance frequency) or to 8.9 MHz (for Na imaging). Because of experimental constraints, only Na and H concentration in solution can be measured. Therefore, evolution of salt concentration within the pores in the presence/absence of 1 mM DTPMP could only be studied for sodium sulfate crystallization (1 M solution).

RESULTS AND DISCUSSION

(a). DTPMP Uptake by Calcite. Figure 1 shows the uptake isotherms of DTPMP on calcite. DTPMP uptake data were fitted both to the traditional Langmuir equation and to a more general Langmuir−Freundlich isotherm:[58]

$$\Gamma_{eq} = \frac{Kq_{max}c^n}{1 + Kc^n} \quad (1)$$

where Γ_{eq} is the adsorbed or uptaken amount of solute, K is the ratio of adsorption (k_a) to desorption (k_d) rate constants, q_{max} is the maximum amount of solute adsorbed, c is solute concentration, and n is a positive coefficient, which indicates the concentration dependence. This latter model yielded a better fit to experimental results than the Langmuir isotherm (Figure 1).

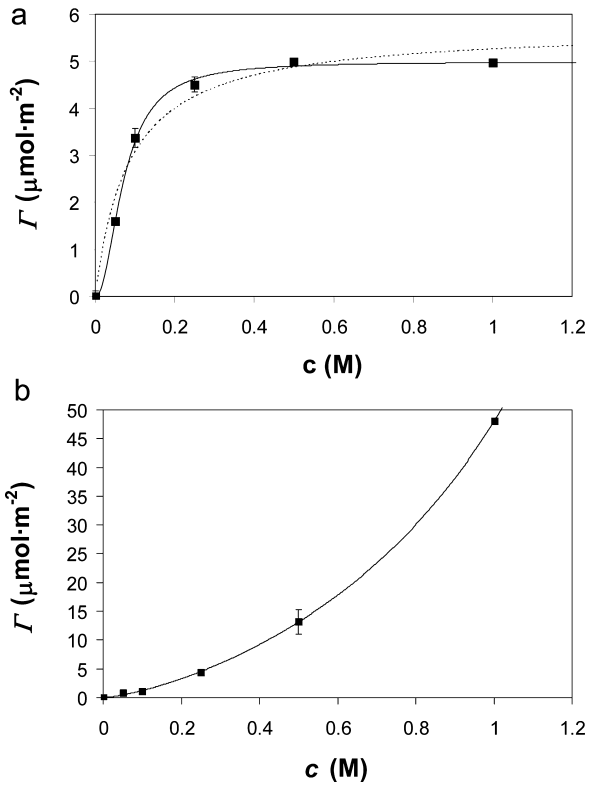

Figure 1. Uptake isotherms of DTPMP on calcite: (a) background electrolyte: 0.1 M $MgSO_4$. Solid line: Langmuir−Freundlich adsorption isotherm; dotted line: Langmuir adsorption isotherm. (b) background electrolyte: 0.1 M Na_2SO_4. Experimental uptake data are fitted to an exponential function (solid line).

Adsorption results were independent of ionic strength both when sodium and magnesium sulfate were used as background electrolytes. DTPMP was found to strongly adsorb onto the crystalline substrate. In the presence of $MgSO_4$, the adsorption isotherm was of type L2 (according to Giles et. al[59,60] classification) and showed a plateau corresponding to ∼5 μmol of DTPMP per m^2 calcite (Figure 1a). This indicates strong attractive forces between adsorbate and substrate, but very weak forces between solute molecules themselves. In contrast, when Na_2SO_4 was the background electrolyte, DTPMP uptake data could not be fitted either to the Langmuir or to the general adsorption isotherm (eq 1). Experimental DTPMP uptake data however showed a good fit to an exponential function (Figure 1b). This is consistent with an irreversible process involving the formation of a surface precipitate, most probably a Ca-phosphonate. The growth of Ca-DTPMP has been previously reported in the literature.[61,62] Kan et. al[63] have shown that two types of Ca- DTPMP salts

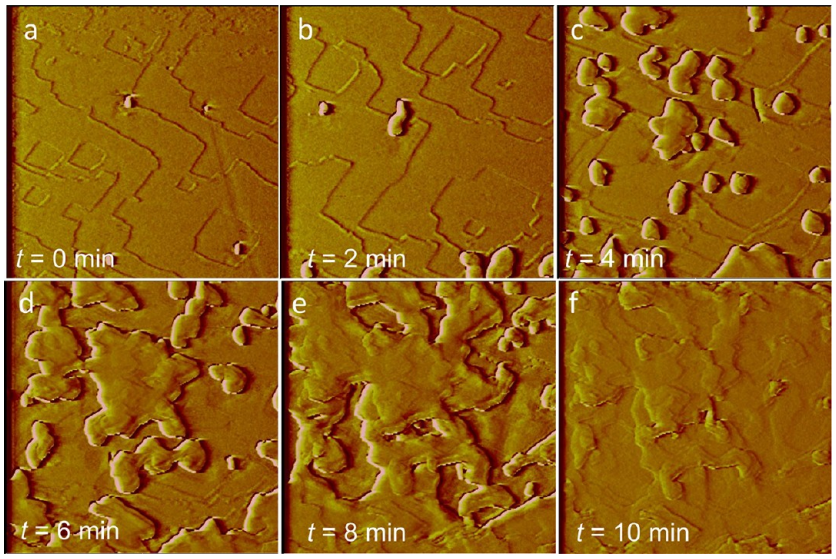

Figure 2. Sequential AFM images of a calcite cleavage surface subjected to sodium sulfate solution flow in the presence of 30 mM DTPMP. AFM deflection images show the initial formation of rhombohedral dissolution pits (a, b) and the formation of a precipitate (Ca-phosphonate), which progressively covers the whole surface as a passivation layer (b–f). The size of each AFM image is 5 × 5 μm.

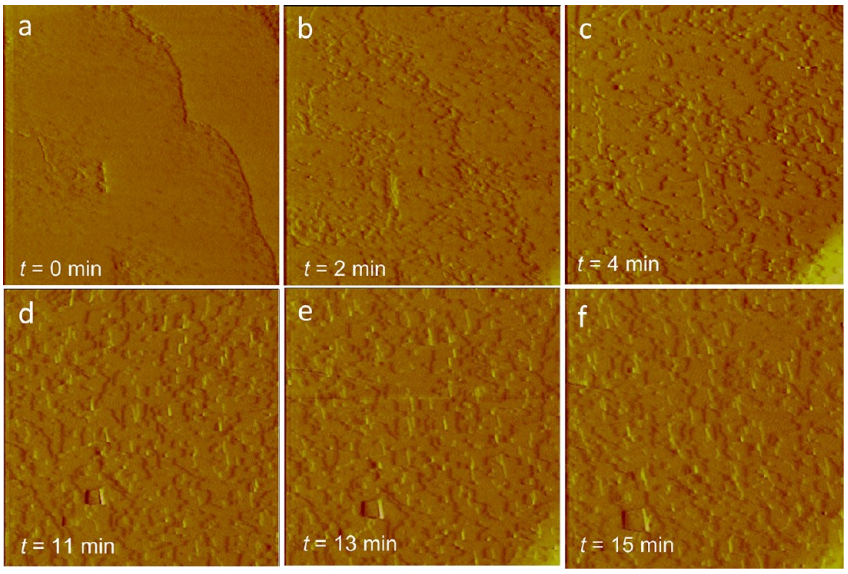

Figure 3. Sequential AFM images of a calcite cleavage surface subjected to magnesium sulfate solution flow in the presence of 30 mM DTPMP. AFM deflection images show the initial formation of abundant rombohedral dissolution pits (a–c) and their limited spreading over time (d–f). No (Mg- or Ca-phosphonate) precipitate is formed. The size of each AFM image is 5 × 5 μm.

(one amorphous and one crystalline) may be formed. We suggest that the precipitate is in this case crystalline as it develops straight edges (seen in the AFM images) that are most likely an indication of the crystalline nature of the new phase formed. It has been shown that saline solutions tend to promote calcite dissolution (salt effect), thus leading to an increased release of Ca^{2+}.[64] DTPMP molecules in solution may thus form Ca-phosphonate complexes. When sufficient supersaturation with respect to Ca-phosphonate is reached, a precipitate will form onto calcite surfaces. This explains the observed exponential rise in the amount of DTPMP removed from the solution. When Mg^{2+} ions are present in solution, Mg^{2+}-phosphonate complexes will form preferentially, thereby preventing or inhibiting precipitation of a Ca-phosphonate. Mg^{2+}-phosphonate complexes are generally more stable and soluble than Ca^{2+}complexes. For instance, the stability constants of Ca^{2+}-HEDP and Mg^{2+}-HEDP are $10^{6.4}$ and $10^{5.7}$, respectively (ionic strength 0.1),[65] while the solubility of phosphonate complexes with alkaline-earth metals increases in the order Ca < Ba < Sr < Mg.[45] Thus, in the presence of magnesium no precipitate will form and phosphonate molecules will adsorb (physisorption) onto calcite surfaces.

(b). In Situ AFM analyses. The initial steps of the interaction between calcite and the sodium sulfate saturated solutions (in the absence and in the presence of DTPMP) were studied at the nanoscale using AFM. When no additive was present, a layer-by-layer dissolution process, similar to that of pure water, was observed and resulted in flatter calcite crystal surfaces. Dissolution features (rhomboedral etch pits) formed on calcite surfaces and rapidly spread and merged to remove a whole $CaCO_3$ layer, followed by the next layer, and so on. However, when DTPMP was added, after an initial period of

dissolution, the precipitation of a thin (~6 nm) layer onto the calcite cleavage plane was observed and it eventually covered the whole surface (Figure 2). This phase was most probably a Ca-phosphonate. This compound is highly insoluble and remained unaltered after the scanning of the surface or the injection of fresh saline solution in the fluid cell. Its formation was fully consistent with our phosphonate adsorption experiments. The precipitation of Ca-phosphonate has been frequently reported in the literature, particularly in the oil industry where phosphonates are used as scale inhibitors and where precipitation squeeze treatments are widely used as a means for their slow release.[48,66−68]

In situ AFM showed the formation of rough (pitted) surfaces following dissolution of calcite by a saturated magnesium sulfate solution.[64] When 30 mM DTPMP was added to the solution, initial dissolution also occurred via the formation of numerous small etch pits, which did not spread significantly over time (Figure 3). In fact, a reduction in etch pit spreading rate from 1.8 to 0.8 nm/s was detected in the presence of DTPMP. Precipitation of new phases (i.e., Ca- or Mg-phosphonate) on the calcite crystal surface was not observed. These observations suggest that adsorption of DTPMP molecules blocks the spreading of etch pits and prevents the formation of new ones. In other words, DPTMP acts as a calcite dissolution inhibitor in this system thus confirming its strong interaction with calcite surfaces as shown by our adsorption experiments. Note that adsorption onto calcite of several organic molecules such as polyacrylates and polyacrylonitrile have been reported to passivate this mineral, thereby presenting a potentially effective method for the protection of carbonate stone against acid attack.[69]

(c). Sodium Sulfate Crystallization in the Presence of DTPMP. ESEM images showed that evaporation of pure solution drops deposited onto calcite surfaces led to randomly oriented precipitation of $Na_2SO_4{\cdot}nH_2O$ (n equal to 7 or 10) crystals (Figure 4a). The formation of hydrated sodium sulfate phases was confirmed by their dehydration following an increase in T of the Peltier stage or a reduction in pH_2O. In the presence of 0.01 M DTPMP two contrasting behaviors were observed. In a set of experiments where pH_2O was reduced at a relatively slow rate, $Na_2SO_4{\cdot}nH_2O$ crystals formed on calcite surfaces. These crystals precipitated in a compact, well-arranged distribution and were attached to the calcite $(10\bar{1}4)$ planes along a well-defined crystallographic plane (Figure 4b). In a second set of experiments where pH_2O was reduced at a relatively fast rate (inducing a fast precipitation event) direct precipitation of thenardite (Na_2SO_4) with rounded, anhedral morphologies occurred (Figure 4c). The phase formed was identified as thenardite because no dehydration occurred when the temperature was increased or pH_2O was reduced in the ESEM chamber. Thenardite crystals aligned parallel to (i) growth steps on calcite $\{10\bar{1}4\}$ surfaces and, (ii) a direction which forms ~73° angle with growth steps. This is close to the angle between $[\bar{4}41]$ direction and its equivalent $[48\bar{1}]$ (75°). The $[\bar{4}41]$ direction corresponds to one of the periodic bond chains (PBCs) of the $\{10\bar{1}4\}$ calcite surface.[70] Direct thenardite crystallization from solution at T < 32.4 °C (i.e., within its metastability field) has been observed during rapid drying (low RH) and has been associated with kinetic effects.[41]

The phase formed in the absence of DTPMP during the in situ XRD experiments was identified as the metastable heptahydrate phase ($Na_2SO_4{\cdot}7H_2O$). This phase rapidly dehydrated into thenardite (Figure 5a). When DTPMP was present, mirabilite crystals precipitated with $(001)_{mirabilite}//$

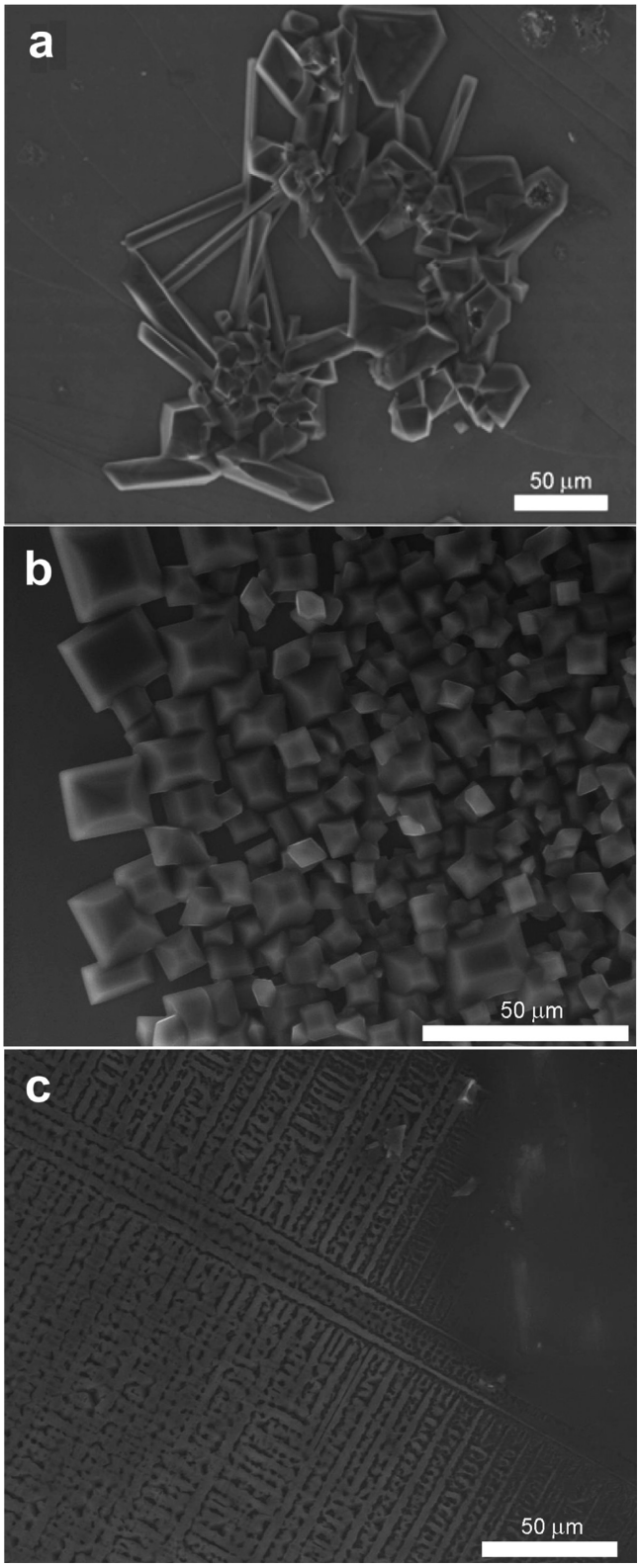

Figure 4. ESEM photomicrographs of sodium sulfate formed on calcite: (a) sodium sulfate hydrate crystals formed in the absence of DTPMP; (b) mirabilite crystals formed in the presence of DTPMP (slow evaporation experiment) with (001) planes parallel to calcite cleavage plane; (c) thenardite crystals formed in the presence of DTPMP aligned along $[\bar{4}41]_{calcite}$.

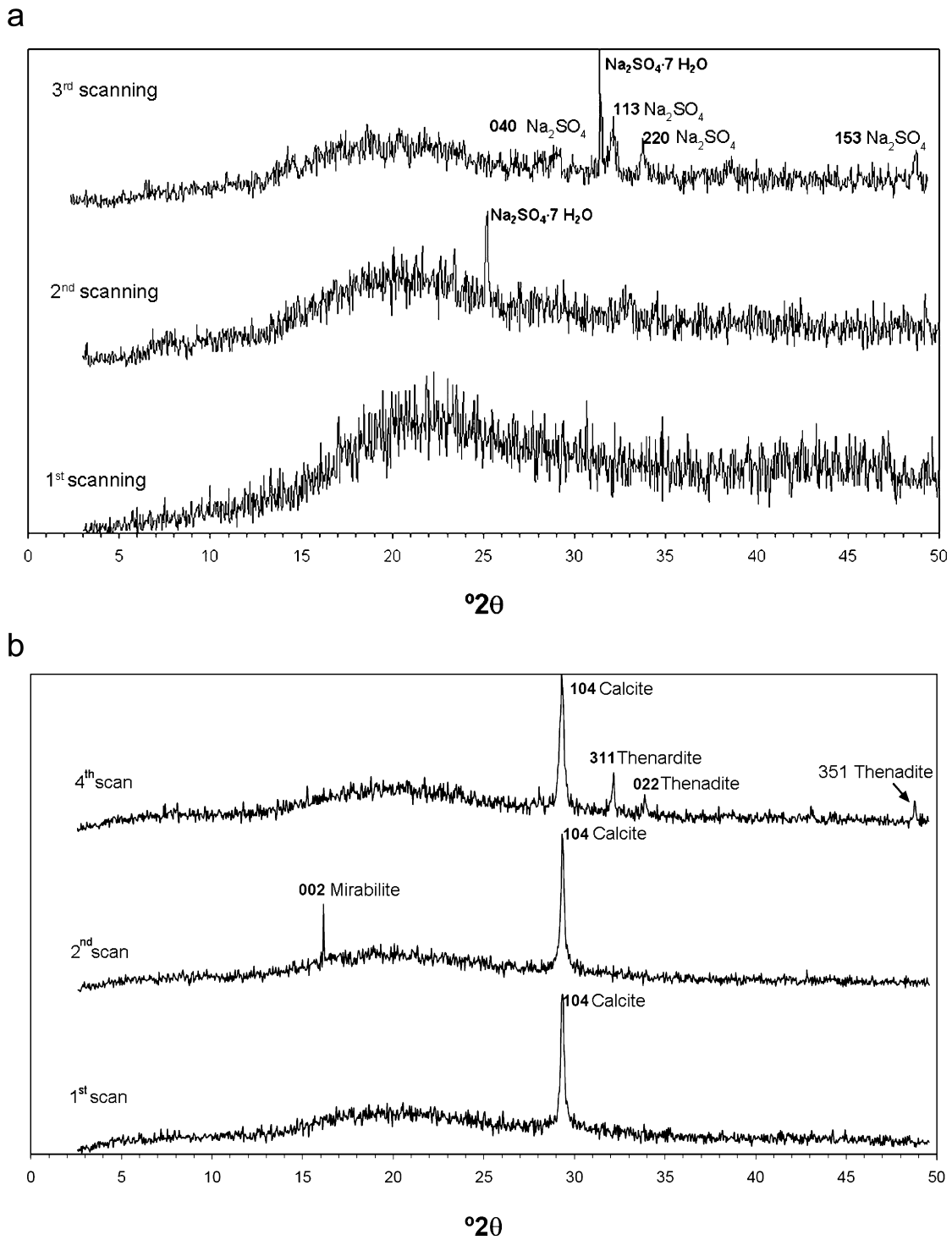

Figure 5. XRD patterns of sodium sulfate crystallization on calcite: (a) in the absence and (b) in the presence of DTPMP. Scan time: 8 min.

$(10\bar{1}4)_{calcite}$ as indicated by the occurrence of an intense $002_{mirabilite}$ Bragg peak (Figure 5b). Using the MSI Cerius[2] software, the morphology of mirabilite crystals was simulated by reducing the growth rate of (001) planes (calculated using BFDH algorithm). The morphology thus obtained was very similar to that observed in situ in the ESEM experiments (Figure 6a,b). The combined results of the XRD analysis and the morphology simulation show that the hydrated phase formed in the presence of DTPMP in the in situ ESEM experiments is, in fact, mirabilite with (001) faces aligned parallel to $(10\bar{1}4)$ calcite planes. Subsequently, mirabilite crystals dehydrated giving rise to randomly oriented thenardite crystals. This is shown by the XRD pattern in which thenardite Bragg peaks intensities correspond to those of a randomly oriented powder sample (JPDFC 37-1465).

Overall, these results show that oriented crystallization of sodium sulfate occurs in the presence of DTPMP, an effect that is not observed in the absence of the additive. This could be due to 2D-heterogeneous nucleation of mirabilite onto the substrate mediated by a thin layer of a Ca-phosphonate precipitate on $\{10\bar{1}4\}$ calcite surfaces. In the case of mirabilite, crystals grew onto this organic precipitate with $\{001\}_{mirabilite}$

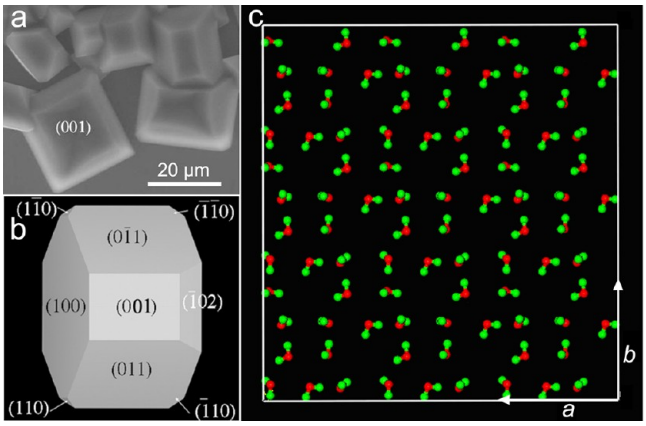

Figure 6. Mirabilite crystals with their (001) planes aligned on Iceland spar (a) and their morphology simulated using the BFDH algorithm (b). Projection of the mirabilite structure along [001] showing the distribution of water molecules in the (001) plane (c) (three unit cells are shown).

parallel to {10$\bar{1}$4} calcite, as shown by XRD. $\{001\}_{mirabilite}$ are the planes of highest water molecule density in mirabilite (Figure 6c), so they offer the highest number of possibilities for H-bonding with deprotonated functional groups of DTPMP. This mechanism seems to control the interaction between DTPMP and this sodium sulfate hydrate phase. Because in this case heterogeneous nucleation is favored, the solution concentration reached at the onset of crystallization is not enough to reach the solubility curve of sodium sulfate heptahydrate,[40] thus preventing its crystallization (see below). Conversely, in the absence of DTPMP no preferential orientation of sodium sulfate hydrate crystals on (10$\bar{1}$4) calcite was observed in the ESEM experiments, while XRD results showed that the phase formed was the heptahydrate. These results indicate that no crystallization promotion was associated with the presence of the pure calcite substrate, thus allowing the solution to reach a higher concentration and enabling the precipitation of randomly oriented sodium sulfate heptahydrate crystals. When oriented thenardite was formed, the interaction with the additive may have taken place through electrostatic binding of PO_3^{2-} groups in the additive adsorbed/precipitated onto calcite and Na^+ cations on Na_2SO_4 faces. Comparing the Na−Na distances in different thenardite faces and the O−O distances in the additive molecules (Table 1), a general high structural fit exists between the additive and the sodium cations

Table 1. Na−Na Distances (Å) in Different (*hkl*) Planes of Thenardite and O−O Distances in PO_3^{-2} Groups of DTPMP^{-8}[a]

(*hkl*)	thenardite	DTPMP^{8-}
(010)	3.167	3.179
	3.712	5.815
	5.719	
(111)	5.719	5.815
	6.815	6.843
	9.815	9.754
(011)	4.200	
	5.863	5.812
	5.901	5.815
	9.815	9.754

[a]Only O−O distances with a mismatch <1% are shown.

present in thernardite (010), (111) and (011) faces. The observed alignment of thenardite crystals parallel to PBCs on (10$\bar{1}$4) calcite planes suggests that additive molecules are adsorbed/precipitated along step edges in these directions. It is suggested that the thin layer of Ca-phosphonate observed with AFM most probably formed epitaxially onto (10$\bar{1}$4) calcite, thereby acting as a "crystallographic bridge" between the substrate and thenardite crystals.

(d). Magnesium Sulfate Crystallization in the Presence of DTPMP. Similar results regarding the oriented precipitation of crystalline phases in the presence of the organic compound were found for magnesium sulfate. In this case, details of the crystallization onto calcite single crystals could not be directly observed in the ESEM, as precipitates formed sub-micrometer crystalline aggregates, thus precluding the identification of individual crystals.[50] In situ XRD experiments were carried out at two different ambient conditions. At relatively high temperature and low relative humidity (25 °C and 40% RH), the direct precipitation of hexahydrite onto {10$\bar{1}$4} surfaces of cleaved Iceland spar crystals was observed, both in the absence (Figure 7a) and in the presence of the additive (Figure 7b). Hexahydrite crystals oriented with {$\bar{4}$11} planes parallel to the calcite cleavage plane when DTPMP was present. This is shown by the relative increase in the intensity of the corresponding Bragg peak. At a lower temperature and higher relative humidity (16 °C and 50% HR), direct precipitation of epsomite was observed, both in the absence (Figure 7c) and in the presence of the additive (Figure 7d). In the first case, the XRD pattern was quite similar to that of a randomly oriented epsomite powder, which suggests that there is no preferential alignment of $MgSO_4{\cdot}7H_2O$ crystals on $(10\bar{1}4)_{calcite}$. When epsomite crystallized in the presence of DTPMP, an important increase in the relative intensity of the $020_{epsomite}$ Bragg peak was observed. This indicates that $MgSO_4{\cdot}7H_2O$ crystals precipitated onto Iceland spar crystals with their (010) planes parallel to {10$\bar{1}$4} calcite surfaces. All in all, these results suggest that adsorbed DTPMP molecules direct both hexahydrite and epsomite oriented crystallization. Apparently, the interaction between the additive and hydrated magnesium sulfates is not highly specific and must take place through the formation of hydrogen bonds between functional groups in the additive adsorbed onto calcite and structural water molecules in the magnesium sulfate crystals. In the case of hexahydrite, ($\bar{4}$11) planes show a high density of water molecules. This is also valid for (010) epsomite planes.[52] This makes these planes ideal for additive-salt crystal interaction.

(e). Model for Salt−Organic Additive−Calcite Interaction. These results allow us to propose a model for the interaction between DTPMP and the salts tested which explains the differential effect of such an additive on sodium and magnesium sulfate crystallization in the absence and in the presence of a calcitic support. It is well-known that polyelectrolytes and several organic molecules are able to act both as crystallization inhibitors when they are in solution and as promoters when they are adsorbed on a substrate.[16] This is the case for DTPMP, which acts as an epsomite and mirabilite crystallization inhibitor when it is free in solution due to its structural affinity with both phases.[44,52] In constrast, when a calcitic support is present, DTPMP is uptaken by calcite surfaces (with or without the formation of a Ca-phosphonate precipitate), leading to changes in the interaction and structural match between the substrate and the nucleating salt. Because of

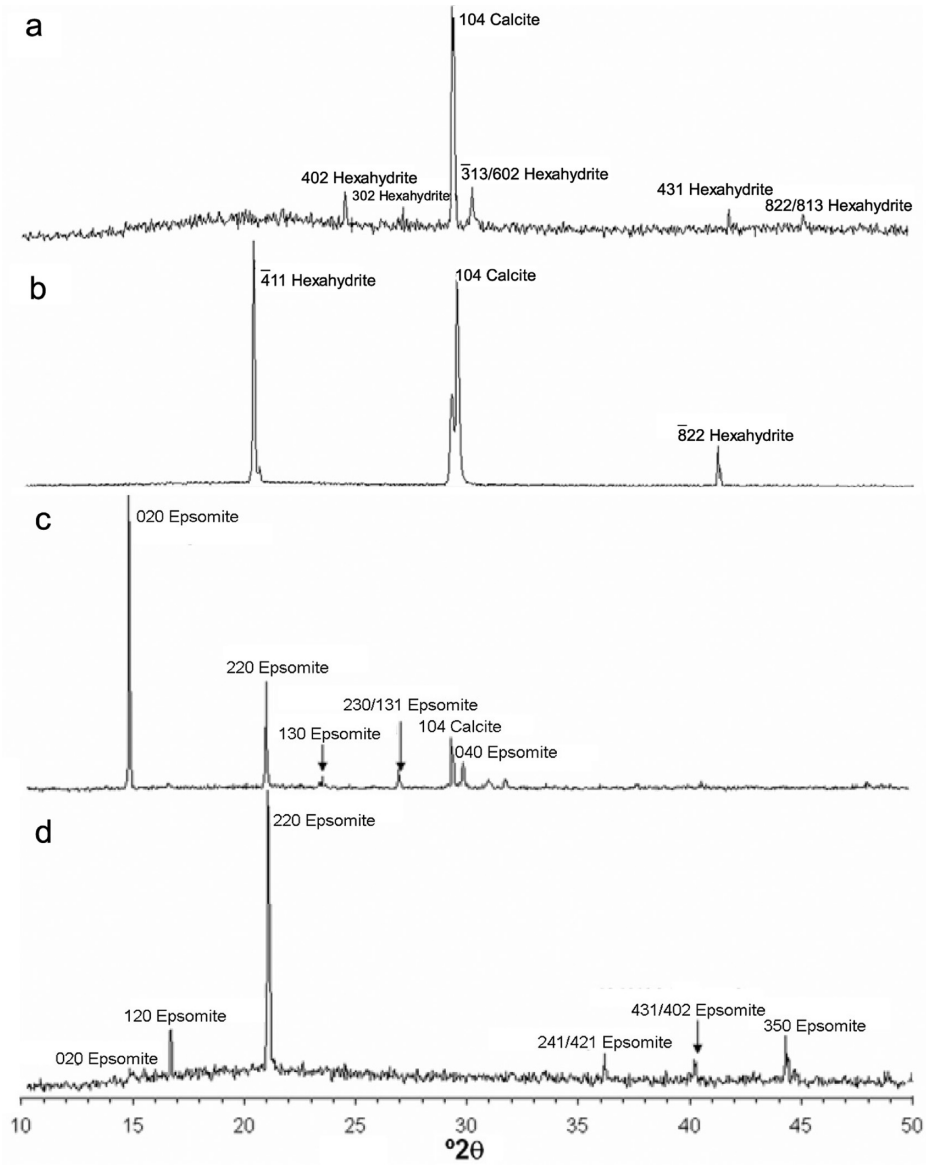

Figure 7. XRD patterns of magnesium sulfate crystallization on calcite cleavage faces: (a) crystallization of hexahydrite at 25 °C and 40% RH in the absence and (b) in the presence of DTPMP. Note that high intensity $\bar{4}11_{hexahydrite}$ Bragg peak in the presence of DTPMP; (c) epsomite crystallization at 16 °C and 50% HR in the absence; and (d) in the presence of DTPMP. Note the high intensity of the $020_{epsomite}$ Bragg peak of epsomite formed in the presence of DTPMP.

the high capacity for establishing H-bonding between deprotonated DTPMP molecules and structural water in both epsomite/hexahydrite and mirabilite, it is expected that the uptake of DTPMP by the substrate (calcite) and its bond to the nucleating phase (Na or Mg sulfate) will significantly reduce the crystal−substrate interfacial free energy (γ_{cs}) and make the interfacial free energy equal between the nucleating phase and the solution (γ_{nf}) and the substrate and the solution (γ_{sf}). A similar effect will also account for the heterogeneous oriented nucleation of thenardite, although in this case binding will not occur via H-bonding, but rather through direct interaction between deprotonated phosphonate groups and Na^+ ions in the anhydrous sodium sulfate salt. Effectively, the adsorbed organic molecules lead to a stronger interaction and a better structural fit between calcite and Na and Mg sulfates.[21] This model is very similar to the widely accepted model used to explain heterogeneous oriented nucleation of mineral phases assisted by organic molecules in biomineralization processes[71,72] and template-directed biomimetic mineral precipitation.[73]

(f). Effect of DTPMP on Salt Crystallization within Limestone Pores. A significant reduction in salt-induced crystallization damage (if compared with additive-free control solutions) was observed when sodium sulfate crystallized within the porous stone in the presence of DTPMP (Figure 8a). However, the formation of efflorescence was not observed as expected, according to the results of crystallization tests in nonconfined systems.[52] MIP analysis of stone samples showed that pores were filled with salts after crystallization tests in the presence of DTPMP (data not shown). These results are consistent with the observed promotion effect of such an adsorbed additive on sodium sulfate crystallization. The same effect (damage reduction and pore filling with salt) was observed in the case of magnesium sulfate crystallizing in the presence of DTPMP (Figure 8b). The null effect of the additive as a crystallization inhibitor within porous supports is due to

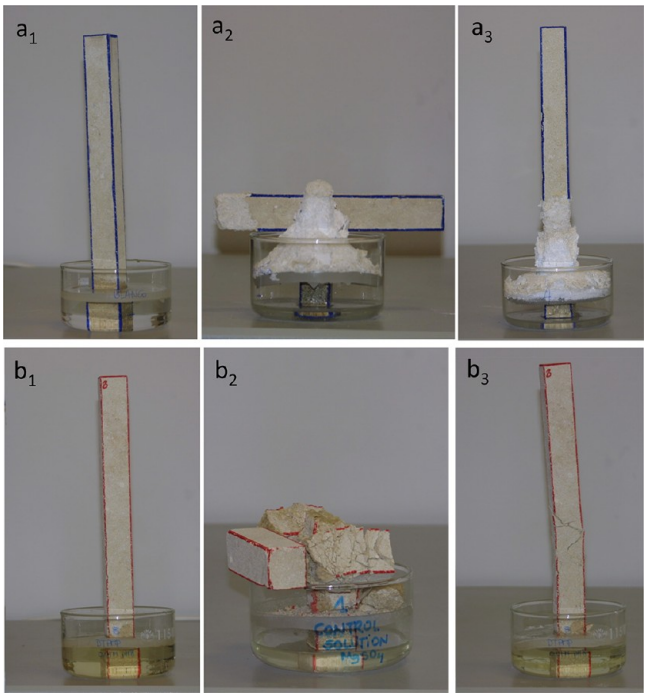

Figure 8. Sequence of images of macroscopic sodium sulfate (a) and magnesium sulfate (b) crystallization tests using limestone slabs: (a1) limestone slab at the beginning of sodium sulfate crystallization test, (a2) limestone slab after 14 days of evaporation of a pure Na_2SO_4 solution, (a3) limestone slab after 14 days of evaporation of Na_2SO_4 solution doped with 0.001 M DTPMP (pH 8); (b1) limestone slab at the beginning of magnesium sulfate crystallization test, (b2) limestone slab after 74 days of evaporation of a pure $MgSO_4$ solution, (b3) limestone slab after 74 days of evaporation of $MgSO_4$ solution doped with 0.001 M DTPMP (pH 8).

the strong tendency of phosphonates to absorb/precipitate on calcite surfaces. As shown above, DTPMP adsorption on calcite prompts a stronger interaction and a better structural match between calcite surfaces and crystallizing sulfates. This should be reflected in the supersaturation reached within stone pores at the onset of crystallization. Actual supersaturation values within the porous stone subjected to evaporative crystallization of sodium sulfate were determined by NMR. Comparison of moisture profiles within stone slabs indicates that water transport/evaporation rate is reduced, if compared with water, due to the influence of the dissolved salt. However, no influence of the additive on the drying rate was detected (Figure 9a,c). It seems that advection dominates the drying process, as the highest salt concentrations are reached on or just below the stone surface.

In the absence of DTPMP, the concentration at the top of the sample rose just above 3.8 *m* (Figure 9b). This implies a supersaturation, β of 3.58 (β = IAP/k_s, where IAP is the ion activity product and k_s is the solubility product; values calculated according to Steiger and Asmussen[40] with respect to $Na_2SO_4 \cdot 10\ H_2O$ or a β value of 1.37 with respect to $Na_2SO_4 \cdot 7H_2O$ (the solution will be undersaturated with respect to thenardite). In the presence of DTPMP, the highest concentration was reached at a location several millimeters below the stone surface. The concentration at this point was ~2 *m* (Figure 9d), which means a value of $\beta \sim 1.66$ with respect to mirabilite (the solution will be undersaturated with respect to sodium sulfate heptahydrate or thenardite). Therefore, the presence of the additive leads to a significant reduction in the supersaturation reached at the onset of crystallization. This is a consequence of the above-mentioned changes in interfacial free energies (γ_{cs}, γ_{nf}, γ_{sf}), which result in a reduction in the nucleation barrier and, therefore, in an increase in the nucleation rate.[21] The crystallization of sulfates is promoted, thus taking place in a compact and oriented manner (as observed in ESEM and XRD in situ experiments), at a lower supersaturation (as determined by NMR measurements). The crystallization pressure exerted by a salt when it grows in a porous material depends on the supersaturation, pore structure of the support, and the surface energy difference between the crystal and the pore wall.[35,74] A crystal normally repels mineral surfaces due to differences in interfacial free energy which originate the so-called disjoining forces (electrostatic and hydration forces).[75,76] The adsorption of DTPMP results in a reduction in the repulsive forces between the growing crystal and the calcitic surfaces ($\gamma_{nf} \approx \gamma_{sf}$) and therefore lowers the supersaturation (driving force) needed for crystallization to occur. When the supersaturation is reduced, the crystallization pressure is lowered according to the relation between supersaturation and crystallization pressure originally proposed by Correns,[77]

$$\Delta P = \frac{RT}{V_m} \ln(\beta) \tag{2}$$

where R is the gas constant, T is the absolute temperature, and V_m is the molar volume of the salt crystal. Maximum Na molal concentration values determined by means of NMR enabled the calculation of the critical supersaturation and the actual maximum crystallization pressure that can be exerted by mirabilite crystallizing within the porous limestone using the equation proposed by Steiger and equation proposed by Steiger and Asmussen:[40]

$$\Delta P = \frac{3RT}{V_m}\left(\ln \frac{m}{m_0} + \ln \frac{\gamma_\pm}{\gamma_{\pm,0}} + \frac{\nu_0}{3} \ln \frac{a_w}{a_{w,0}}\right) \tag{3}$$

where m_0, $\gamma_{\pm,0}$ and $a_{w,0}$ refer to the molality, the mean activity coefficient and the water activity of the respective saturated solutions, ν_0 takes a value of 10 for mirabilite, and V_m of mirabilite is 219.8 $cm^3\ mol^{-1}$. Equation 3 yields ΔP values of 14.1 and 5.6 MPa in the case of mirabilite crystallization in the absence and in the presence of DTPMP (at 20 °C). These results show that a significant reduction in crystallization pressure is associated with the presence of DTPMP on calcite surfaces. According to Hamilton et al.,[78] the effective crystallization stress associated with salt crystallization in a porous material is, to a first approximation, $\phi\Delta P$ where ϕ is the volume fraction of mirabilite in the bulk material. Considering that the pore fraction of the tested limestone is ~0.3 (from MIP results), the maximum volume fraction of mirabilite would be 0.3. Thus, the effective stresses are 4.23 and 1.68 MPa in the case of mirabilite crystallization in the absence and in the presence of DTPMP. The tensile strength of the tested limestone is 1.8 ± 0.5 MPa.[79] Salt damage occurs when the effective stress due to generation of salt crystallization pressure in a porous material is higher than the tensile stress.[78,80] It follows that the reduction in crystallization pressure associated with the presence of DTPMP explains the reduction in damage to the porous stone support observed in our macroscale salt crystallization tests. Although our XRD results show that

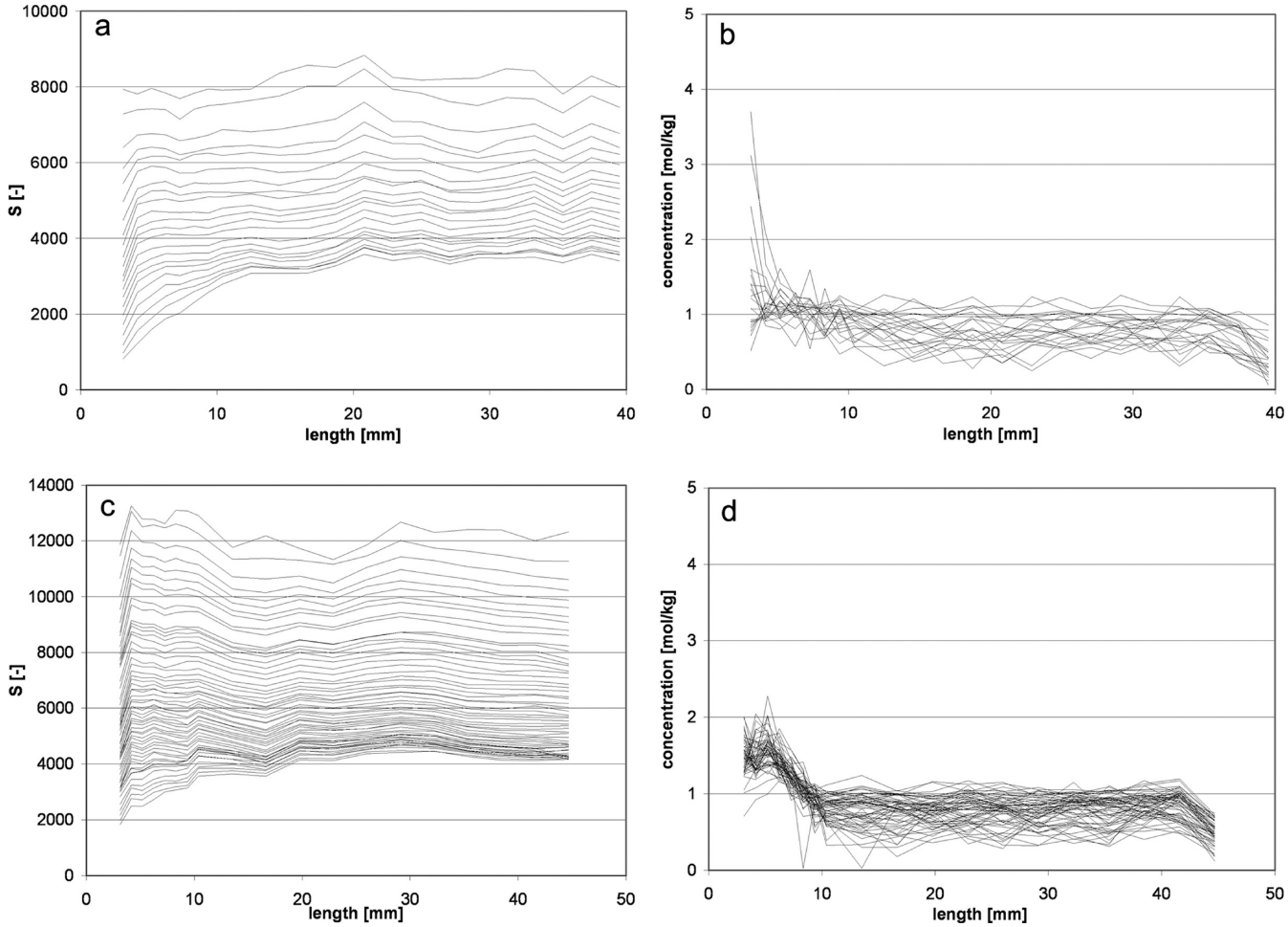

Figure 9. Moisture (s, arbitrary units) (a and d) and salt concentration (b and d) time evolution vs probe length (i.e., depth within a stone block) during drying of limestone samples laden with 1 M Na_2SO_4 (a, b) and 1 M Na_2SO_4 + 0.001 M DTPMP (c, d). Profiles were measured every two hours by NMR.

sodium sulfate heptahydrate can form directly on calcite single crystals in the absence of DTPMP, its direct crystallization limestone cannot account for the damage observed during crystallization tests.[81] If we assume heptahydrate precipitation, the supersaturation reached at the onset of crystallization determined by NMR will lead to a ΔP value of 1.29 MPa, and an effective stress of only 0.38 MPa. Such a very low effective stress does not explain the significant damage observed following macroscale sodium sulfate crystallization within the limestone blocks in the absence of DTPMP (Figure 8a). Differences in evaporation dynamics/kinetics and possible metastable−stable phase transitions in a porous material[81] may explain the differences observed when comparing crystallization in a porous stone with crystallization on an unconstrained calcite single crystal surface.

The damage reduction experienced by the limestone blocks subjected to magnesium sulfate crystallization in the presence of DTPMP can be explained by a similar mechanism as that proposed for the case of sodium sulfate. Unfortunately, the technical limitations of NMR precluded the evaluation of the Mg concentration at the onset of crystallization, so we could not calculate the critical supersaturation and associated crystallization pressure of magnesium sulfate salts formed in the pores of the limestone.

■ CONCLUSIONS

The crystallization of sodium and magnesium sulfates on calcite supports in the presence of DTPMP is explained by a model based on the formation of an organophosphonate template which directs sulfate crystallization. Randomly deposited crystals of a hydrated sodium sulfate phase ($Na_2SO_4{\cdot}7H_2O$) were observed in ESEM and XRD crystallization experiments performed in the absence of phosphonate. Oriented and compact mirabilite and thenardite crystals precipitate onto $\{10\bar{1}4\}$ calcite surfaces in the presence of DTPMP during in situ crystallization experiments. ESEM and XRD results show that (001) mirabilite faces align parallel to cleavage planes of Iceland Spar crystals. In the case of magnesium sulfate, hexahydrite or epsomite (depending on the ambient conditions) crystallizes randomly when growth takes place from pure solution and with faces oriented parallel to $(10\bar{1}4)$ calcite planes in the presence of DTPMP. Adsorbed DTPMP molecules, which form a template on calcite surfaces, can suppress the crystallographic mismatch between sulfate crystals and the calcitic substrate, and promote the formation of oriented sulfate crystal assemblies. The formation of such an organic template contributes to the heterogeneous nucleation of mirabilite ($Na_2SO_4{\cdot}10H_2O$) within a porous limestone at a low supersaturation (if compared with the crystallization in the absence of additive), as shown by NMR measurements. Similar

results are expected for magnesium sulfate, although in this case supersaturation measurements could not be performed due to experimental constraints of our NMR equipment. The observed crystallization promotion effect significantly reduces crystallization pressure exerted by these salts when growing within a porous calcitic substrate (limestone), thereby reducing salt damage as observed in macroscale salt weathering tests. It is therefore suggested that crystallization promoters such as DTPMP may help minimize damage to porous carbonate stones due to salt crystallization, which is one of the main hazards for historic architecture and statuary. Because adsorbed/precipitated phosphonate passivates the surface of calcite, application of this type of additive may also reduce chemical weathering of carbonate stones. However, the possibility that damage due to other mechanisms such as the thermal expansion mismatch between the stone and the salt filling the pores cannot be ruled out and should be checked in future studies. These results also suggest that the extensive use of phosphonates as crystallization inhibitors to prevent pore plugging due to Ca and Ba sulfate crystallization in oil fields could in fact enhance such a problem in carbonate reservoir rocks due to template-assisted sulfate precipitation.

■ AUTHOR INFORMATION

Corresponding Author

*E-mail: encaruiz@ugr.es; tel: +34 958 240 473; fax: +34 958 243 368.

Notes

The authors declare no competing financial interest.

■ ACKNOWLEDGMENTS

This research was financed by the European Commission VIth Framework Program (Contract No. SSP1-CT-2003-501571), the Spanish Government (Grant MAT2009-11332) and the Junta de Andalucía (Research Group RNM-179 and Project P11-RNM-7550). E.R.-A. also acknowledges the receipt of a Ramón y Cajal grant from Spanish Ministry of Economy and Competitivy. ESEM analyses were performed at The Getty Conservation Institute (Los Angeles, USA) and AFM experiments at the Institut für Mineralogie, Münster, (Germany), where the research facilities are supported by the DFG (German Research Foundation).

■ REFERENCES

(1) Mullin, J. W. *Crystallization*; Butterwoth-Heinemann: Oxford, 1992.
(2) van Rosmalen, G. M. *Chem. Eng. Commun.* **1983**, *20*, 209−233.
(3) Cody, A,M.; Cody, R. D. *J. Cryst. Growth* **1991**, *113*, 508−519.
(4) Füredi-Milhofer, H.; Sarig., S. *Prog. Cryst. Growth Ch.* **1996**, *32*, 45−74.
(5) Veintemillas-Verdaguer, S. *Prog. Cryst. Growth Ch.* **1996**, *32*, 75−109.
(6) Zhang, D.; Qi, L.; Ma, J.; Cheng, H. *Chem. Mater.* **2002**, *14*, 2450−2457.
(7) Al-Jibbouri, S.; Ulrich, J. *Cryst. Res. Technol.* **2004**, *39*, 540−547.
(8) Sommerdijk, N. A. J. M.; de With, G. *Chem. Rev.* **2008**, *108*, 4499−4550.
(9) Austin, A. E.; Miller, J. F.; Vaughan, D. A.; Kircher, J. F. *Desalination* **1975**, *16*, 345−357.
(10) Black, S. N.; Bromley, L. A.; Cottier, D.; Davey, R. J.; Dobbs, B.; Rout, J. E. *J. Chem. Soc. Faraday T.* **1991**, *87*, 3409−3414.
(11) Lowenstam, H. A.; Weiner, S. *On Biomineralization*; Oxford University Press: Oxford, 1989.
(12) Mann, S. *Biomineralization: Principle and Concepts in Bioinorganic Materials Chemistry*; Oxford University Press: Oxford, 2001.
(13) Qiu, S.r.; Wierzbicki, A.; Orme, C. A.; Cody, A. M.; Hoyer, J. R.; Nancollas, G. H.; Zepeda, S.; De Yoreo, J. J. *Proc. Natl. Acad. Sci. U. S. A.* **2004**, *101*, 1811−1815.
(14) Sheng, X.; Jung, T.; Wesson, J. A.; Ward, M. D. *Proc. Natl. Acad. Sci. U. S. A.* **2005**, *102*, 267−272.
(15) Meldrum, F. C.; Cölfen, H. *Chem. Rev.* **2008**, *108*, 4332−4432.
(16) Campbell, A. A.; Ebrahimpour, A.; Perez, L.; Smesko, S. A.; Nancollas, G. H. *Calcified Tissue Int.* **1989**, *45*, 122−128.
(17) Bayton, A.; Chandler, B. D.; Jones, F.; Nealon, G.; Ogden, M. I.; Radomirovic, T.; Shimizu, G. K. H.; Taylor, J. M. *CrystEngComm* **2011**, *13*, 1090−1095.
(18) Liu, X. Y. *J. Cryst. Growth* **2002**, *237−239*, 1806−1812.
(19) Buckley, H. E. *Disc. Faraday Soc.* **1949**, *5*, 243−254.
(20) Nancollas, G. H.; Zawacki, S. J. *Ind. Cryst.* **1984**, *84*, 51−59.
(21) Liu, X. Y. *J. Phys. Chem. B* **2001**, *105*, 11550−11558.
(22) Bosbach, D.; Coveney, P. V.; Griffin, J. L. W.; Putnis, A.; Risthaus, P.; Stackhouse, S.; Whiting, A. *J. Chem. Soc. Perkin Trans.* **2002**, *2*, 1238−1245.
(23) Lupu, C.; Arvidson, R. S.; Lüttge, A.; Barron, A. R. *Chem. Commun.* **2005**, *18*, 2354−2356.
(24) Badens, E.; Veesler, S.; Boistelle, R. *J. Cryst. Growth* **1999**, *198/199*, 704−709.
(25) Liu, X. Y. In *Nanoscale Structure and Assembly at Solid-Fluid Interfaces. Vol. 1, Interfacial Structure vs. Dynamics*; Liu, X. Y., De Yoreo, J. J., Eds.; Kluwer Academic Publishers: Norwell, MS, 2004; pp 109−176.
(26) Heywood, B. R.; Mann, S. *Adv. Mater.* **1994**, *6*, 9−20.
(27) Mertig, M.; Seidel, R.; Colombi Ciacchi, L.; Pompe, W. *AIP Conference Proceedings* **2002**, *633*, 449−453.
(28) Wu, Q.; Zheng, N.; Ding, Y.; Li, Y. *Inorg. Chem. Commun.* **2002**, *5*, 671−673.
(29) Mann, S.; Ozin, G. A. *Nature* **1996**, *382*, 313−318.
(30) Li, C.; Kaplan, D. L. *Curr. Opin. Solid State Mater. Sci.* **2003**, *7*, 265−271.
(31) Fricke, M.; Volkmer, D. *Top. Curr. Chem.* **2007**, *270*, 1−41.
(32) Xu, A.-W.; Ma, Y.; Cölfen, H. *J. Mater. Chem.* **2007**, *17*, 415−449.
(33) Gower, L. B. *Chem. Rev.* **2008**, *108*, 4551−4627.
(34) Winkler, E. M.; Singer, P. C. *Geol. Soc. Am. Bull.* **1972**, *83*, 3509−3513.
(35) Espinosa-Marzal, R. M.; Scherer, G. W. *Acc. Chem. Res.* **2010**, *43*, 897−905.
(36) Evans, I. S. *Rev. Geomorphol. Dyn.* **1970**, *19*, 153−177.
(37) Winkler, E. M. *Stone in Architecture, Properties and Durability*; Springer, Berlin Heidelberg: New York, 1994.
(38) Goudie, A. S.; Viles, H. A.; Parker, A. G. *J. Arid Environ.* **1997**, *37*, 581−598.
(39) Rodríguez-Navarro, C.; Doehne, E. *Earth Surf. Processes Landforms* **1999**, *24*, 191−209.
(40) Steiger, M.; Asmussen, S. *Geochim. Cosmochim. Acta* **2008**, *72*, 4291−4306.
(41) Rodríguez-Navarro, C.; Doehne, E.; Sebastian, E. *Langmuir* **2000**, *16*, 947−954.
(42) Selwitz, C.; Doehne, E. *J. Cult. Herit.* **2002**, *3*, 205−216.
(43) Rodriguez-Navarro, C.; Linares-Fernandez, L.; Doehne, E.; Sebastián, E. *J. Cryst. Growth* **2002**, *243*, 503−516.
(44) Ruiz-Agudo, E.; Rodriguez-Navarro, C.; Sebastian-Pardo, E. *Cryst. Growth Des.* **2006**, *6*, 1575−1583.
(45) Nowack, B. *Water Res.* **2003**, *37*, 2533−2546.
(46) Nowack, B.; Stone, A. T. *J. Colloid Interface Sci.* **1999**, *214*, 20−30.
(47) Weijnen, M. P. C.; Van Rosmalen, G. M. *J. Cryst. Growth* **1986**, *79*, 157−168.
(48) Pairat, R.; Sumeath, C.; Browning, F. H.; Fogler, H. S. *Langmuir* **1997**, *13*, 1971−1798.
(49) Goudie, A.; Viles, H. *Salt Weathering Hazards*; Wiley: Chichester, 1997.

(50) Ruiz-Agudo, E.; Mees, F.; Jacob, P.; Rodriguez-Navarro, C. *Environ. Geol.* **2007**, *52*, 269−281.
(51) ASTM C 88−90, Standard test method for soundness of aggregate by use of sodium sulfate or magnesium sulfate. In *Annual Book of ASTM Standards*; ASTM: Philadelphia, PA, 1997; Vol. *4*, Chapter 2, pp 37−42.
(52) Ruiz-Agudo, E.; Putnis, C. V.; Rodriguez-Navarro, C. *Cryst. Growth Des.* **2008**, *8*, 2665−2673.
(53) Xyla, A. G.; Mikroyannidis, J.; Koutsoukos, P. G. *J. Colloid Interface Sci.* **1992**, *153*, 537−551.
(54) Grasshoff, K.; Ehrhardt, M.; Kremling, K. *Methods of Seawater Analysis*; Verlag Chemie: Nurnberg, 1983.
(55) Parkhurst, D. L.; Appelo, C. A. J. *U.S. Geological Survey Water-Resources Investigation Report 99−4259* **1999**, 312.
(56) Arvidson, R. S.; Collier, M.; Davis, K. J.; Vinson, M. D.; Amonette, J. E.; Luttge, A. *Geochim. Cosmochim. Acta* **2006**, *70*, 583−594.
(57) Kopinga, K.; Pel, L. *Rev. Sci. Instrum.* **1994**, *65*, 3673−3681.
(58) Adamson, A. W. *Physical Chemistry of Surfaces*, 5th ed.; John Wiley & Sons: New York,1990.
(59) Giles, C. H.; Smith, D.; Huitson, A. *J. Colloid Interface Sci.* **1974**, *47*, 755−765.
(60) Giles, C. H.; ÒSilva, A. P.; Easton, I. A. *J. Colloid Interface Sci.* **1974**, *47*, 765−778.
(61) Baraka-Lokmane, S.; Sorbie, K. S. *J. Pet. Sci. Eng.* **2010**, *70*, 10−27.
(62) Zhang, B.; Zhang, L.; Li, F.; Hu, W.; Hannam, P. M. *Corros. Sci.* **2010**, *52*, 3883−3890.
(63) Kan, A. T.; Oddo, J. E.; Tomson, M. B. *Langmuir* **1995**, *10*, 1450−1455.
(64) Ruiz-Agudo, E.; Putnis, C. V.; Jiménez-López, C.; Rodríguez-Navarro, C. *Geochim. Cosmochim. Acta* **2009**, *73*, 3201−3217.
(65) Popov, K.; Rönkkömäki, H.; Lajunen, L. H. J. *Pure Appl. Chem.* **2001**, *73*, 1641−1677.
(66) Browning, F. H.; Fogler, H. S. *Langmuir* **1996**, *11*, 4143−4152.
(67) Tantayakom, V.; Fogler, H. S.; Charoensirithavorn, P.; Chavadej, S. *Cryst. Growth Des.* **2005**, *5*, 329−335.
(68) Ruiz-Agudo, E.; Di Tommaso, D.; Putnis, C. V.; de Leeuw, N. H.; Putnis, A. *Cryst. Growth Des.* **2010**, *10*, 3022−3035.
(69) Thompson, M.; Wilkins, S. J.; Compton, R. G.; Viles, H. A. *J. Colloid Interface Sci.* **2003**, *260*, 204−210.
(70) Paquette, J.; Reeder, R. J. *Geochim. Cosmochim. Acta* **1995**, *59*, 735−749.
(71) Jiang, H. D.; Liu, X. Y.; Zhang, L. Y.; Li, Y. *J. Biol. Chem.* **2005**, *280*, 42061−42066.
(72) Gunthorpe, M. E.; Sikes, C. S.; Wheeler, A. P. *Biol. Bull.* **1990**, *179*, 191−200.
(73) Pouget, E.; Bomans, P..; Goos, J.; Frederik, P. M.; de With, G.; Sommerdijk, N. *Science* **2009**, *323*, 1455−1458.
(74) Rijniers, L. A.; Huinink, H. P.; Pel, L.; Kopinga, K. *Phys. Res. Lett.* **2005**, *94*, 075503.
(75) Scherer, G. W. *Cem. Concr. Res.* **2004**, *34*, 1613−1624.
(76) Houck, J.; Scherer, G. W. In *Fracture and Failure of Natural Building Stones*; Kourkoulis, S. K., Ed.; Springer: Dordrecht, The Netherlands, 2006.
(77) Correns, C. W. *Discuss. Faraday Soc.* **1949**, *5*, 267−271.
(78) Hamilton, A.; Hall, C.; Pel, L. *J. Phys. D: Appl. Phys.* **2008**, *41*, 212002/1−212002/5.
(79) Rodríguez-Navarro, C.; Rodríguez-Navarro, A.; Elert, K.; Sebastian, E. *J. Appl. Phys.* **2004**, *95*, 3350−3357.
(80) Scherer, G. W. In *Proc. 9th Int. Cong. Deterioration and Conservation of Stone*; Fassina, V., Ed.: Elsevier: Amsterdam, 2000; Vol. *1*, pp 187−194.
(81) Schiro, M.; Ruiz-Agudo, E.; Rodriguez-Navarro, C. *Phys. Rev. Lett.*, in press.